Computer simulation of the rheology of grafted chains under shear. II. Depletion of chains at the wall

G. H. Peters
Chemistry Department III, H. C. Ørsted Institutet, University of Copenhagen, Universitetsparken 5, DK-2100 Copenhagen Ø, Denmark and Novo-Nordisk A/S, Novo Allé 1, DK-2880 Bagsvaerd, Denmark

D. J. Tildesley
Department of Chemistry, Imperial College of Science Technology and Medicine, South Kensington London SW7 2AY, United Kingdom
(Received 22 May 1996)

We report nonequilibrium molecular dynamics simulations of grafted and free chains surrounded by solvent molecules and sheared between two atomic walls. Each wall is covered by a layer of amphiphilic molecules, which are twenty units long and chemically bounded to the surface. Simulations were performed at surface coverages ranging from 1/3 to 0, where 1/3 corresponds to a system with only grafted chains. Coverages lower than 1/3 were obtained by randomly detaching chains from the wall. The particles interact through the Weeks-Chandler-Andersen repulsive potential. Bond interactions and the stiffness of the chains are modeled using harmonic potentials. Heat is removed from the system through the walls by applying a Nose-Hoover thermostat. At coverages larger than 0, the chains behave like a wall resulting in steep velocity gradients. With decreasing coverages, the tilt of the amphiphiles is increased, and at the same time solvent molecules diffuse into the chain region. This effect of solvent molecules entering into the chain region is most pronounced at a coverage of 0.22. Frictional forces are higher for the intermediate coverages. This is probably due to entanglements between free and grafted chains. Decreasing the flexibility of the amphiphilic molecules creates a more dramatic response to the imposed shear field resulting in a larger chain tilt, higher frictional forces, and a higher solvent density at the wall. [S1063-651X(96)13711-9]

PACS number(s): 36.20.Fz, 68.15.+e, 36.20.Ey

I. INTRODUCTION

Much of the interest in the rheology of molecularly thin films has been stimulated by experiments conducted to determine frictional forces [1–9]. These experiments revealed that the rheology of nanoscopically thin films of organic lubricants can be drastically different from that of the corresponding bulk liquids. A detailed understanding of the properties of liquids in a confined geometry and of the physical origin of these confinement induced changes is fundamentally important to basic and applied problems such as adhesion, capillarity, contact formation, friction, lubrication, wear, modifications of surfaces, etc. [10–21]. Theoretical approaches [22,23] and simulation techniques (in particular with the recent developments in computer hardware and implementations of computational methods) [24–53] have been used to elucidate the microscopic origins for these phenomena and their technological consequences.

Many modern instruments require smooth, low-friction surfaces to reduce wear and increase equipment lifetime. Especially with the production of miniature motors and aerospace devices, this area has become the subject of intense activity and recent approaches have focused on boundary lubrication processes, where graphite, inorganic compounds, or amphiphilic molecules are adsorbed at the solid surface to reduce friction and wear between sliding surfaces. For such a system, the friction between the pure surfaces is replaced by the weaker adhesive contact forces between the lubricant layers. Macroscopically, friction is accompanied by conductive heat flow and several studies have investigated the mechanism by which the system dissipates energy using first principles calculations [29,30] based on *ab initio* total energy calculations of moving two layers past each other or by molecular dynamics simulations [31–33].

Most of the computational studies were performed using traditional atomic-scale modeling of atoms and molecules, which allows us to consider relatively small systems and short times. We have used mesoscale computer modeling [34], which significantly reduces the computational burden and provides an avenue to extend simulation periods up to several nanoseconds. Additionally, these methods allow us to study collective and cooperative behavior such as phase separations, the formation of micelles, and viscoelasticity [35–48].

In our first paper [53] we investigated structural and rheological properties of grafted amphiphiles at a range of reduced shear rates varying from 0.0 to 0.101. Interestingly, we found that the grafted chains behave like a wall that was displaced into the flow a distance corresponding to the hydrodynamic thickness of the layer. Due to the shear induced flow and hence the flow resistance, the grafted amphiphilic molecules tilted, and this was accompanied by an elongation of the chains. During shearing, solvent molecules are expelled from the chain region close to the boundary wall. Increasing the stiffness of the chains produced significant changes in their geometry, but only affected the flow behavior slightly.

In the present study, we have varied the surface coverage by randomly detaching amphiphiles from the wall, a process that is encountered, for instance, in surface force apparatus when studying frictional forces between solid surfaces coated with polymer brushes [8]. We are interested in how the shearing and detachment of surfactant molecules change the structural characteristics and rheological properties of the system. Throughout the simulations, we applied a reduced

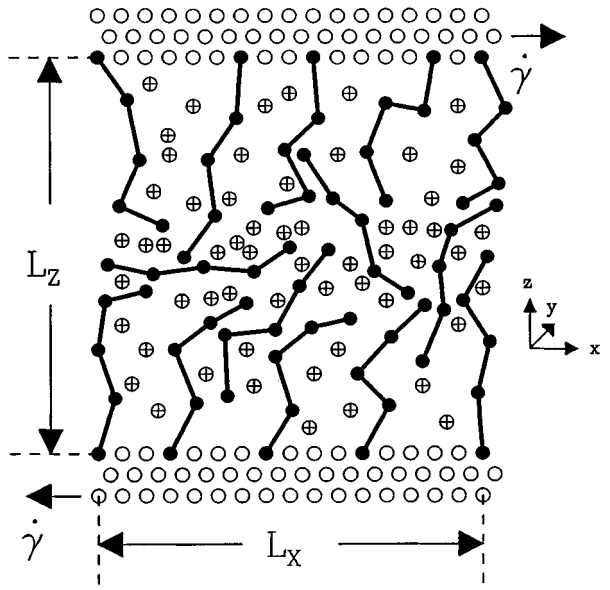

FIG. 1. Schematic representation of the simulation cell. Open, marked with a cross, and filled circles represent boundary, fluid, and chain particles. $\dot{\gamma}$ indicates the direction of the displacement of the wall particles to impose a shear field on the fluid.

shear rate of 0.0101, which in the case of block polymers assuming that each unit is of size 100 Å with an average mass of 50 000 g/mol corresponds to a shear rate of the order of 10^{-3} ns^{-1}. Typical shear rates observed in experiments are in the range of 10^{-7}–10^{-4} ns^{-1} in surface force apparatus [5,49]. Similar rates are proposed for spontaneous shape changes in bilayers leading to a significant increase in curvature [50]. Though our shear rate is slightly higher, it was determined by the results of our previous study [53], where we observed that lower rates yielded pressure tensor and viscosity data with large uncertainties (low signal to noise ratio).

The paper is organized as follows. In Sec. II we describe the potential model and simulation details used in our shearing experiments. Section III contains a discussion of our results obtained for different surface coverages of flexible and stiff amphiphilic molecules immersed in Lennard-Jones fluid and free amphiphiles. Finally, we conclude by summarizing the changes of the rheological properties observed due to detachment of amphiphiles and the effect of increasing chain stiffness.

II. MODEL AND SIMULATION

The model used in our computational study and displayed in Fig. 1 is composed of solvent molecules, amphiphilic chains, and two atomic boundary walls. The chains can be grafted to the wall or free to move in the solvent. The interaction between all particles is described by a shifted and truncated Lennard-Jones potential known as the repulsive Weeks-Chandler-Andersen potential (WCA) [51] and is given by

$$U_{\mathrm{LJ}}=4\epsilon\left[\left(\frac{\sigma}{r}\right)^{12}-\left(\frac{\sigma}{r}\right)^{6}\right]+\epsilon, \quad r\leqslant 2^{1/6}, \tag{1}$$

$$U_{\mathrm{LJ}}=0, \quad r>2^{1/6}, \tag{2}$$

where σ and ϵ are the collision diameter and the well depth of the potential, respectively. This potential is truncated and shifted at the minimum of the full Lennard-Jones potential and only includes repulsive contributions. Additional attractive potentials are required for the bead-bead interaction in the chains and to keep certain particles in the crystal lattice that forms the wall. The intramolecular bead interactions are modeled by the bead spring potential [44], where beads are connected by an anharmonic spring [45–47] of the form

$$U_c=-\frac{1}{2}k_cR_0^2\ln\left[1-\left(\frac{r}{R_0}\right)^2\right], \quad r\leqslant R_0, \tag{3}$$

$$U_c=\infty, \quad r>R_0. \tag{4}$$

The adopted values for k_c and R_o are $30\epsilon/\sigma^2$ and 1.5σ and are taken from Ref. [47].

The stiffness of the chains is controlled by including one additional harmonic potential acting between beads i and $i+2$,

$$U_{bd,ik}=\frac{1}{2}k_{ik}(|\vec{r}_{ik}-\vec{r}_{eq.,ik}|)^2, \quad k=i+2 \tag{5}$$

with $\vec{r}_{eq.,ik}=1.9216\sigma$, which is twice the distance of the location of the minimum of the potential given by Eqs. (1)–(4). The force constant k_{ik} is equal to k_c defined above. Two sets of simulations were performed using ($k_{ik}=0$) and ($k_{ik}=30$). Henceforth, these two sets of parameter are referred to as LJ+C (Lennard-Jones plus chains) and LJ+SC (Lennard-Jones plus stiff chains).

The wall atoms are attached to their initial lattice points, $\vec{r}_{eq,i}$, by a harmonic potential

$$U_{bd,w}=\frac{1}{2}k_w(|\vec{r}_i-\vec{r}_{eq,i}|)^2. \tag{6}$$

The force constant, $k_w=72\epsilon/(2^{1/3}\sigma^2)$, is equal to the numerical value of the second derivative of the full Lennard-Jones potential determined at the minimum of the potential [25]. This yields a harmonic potential well, which is comparable to the full LJ potential [26]. It is sufficiently deep to prevent the wall atoms from moving from their equilibrium positions, and at the same time provide a thermal bath for removing heat from the system and preventing solvent molecules from entering the wall region. Each wall contains 306 particles arranged in three hexagonally close packed layers. In view of the short range nature of the WCA potential, the boundary is sufficiently thick that solvent particles which are trapped close to the walls do not experience a direct force from the outermost layer.

The nonequilibrium molecular dynamics (NEMD) simulations [52–58] were performed in an orthorhombic cell with periodic boundary conditions applied in the x and y directions. Along the z direction, the fluid is bound by the two walls. The cell dimensions L are in reduced units: $L_x=17.0$, $L_y=5.83$, and $L_z=33.80$. The initial configuration was generated by randomly tethering amphiphilic molecules of chain length 20 beads to each wall corresponding

TABLE I. Simulation details. LJ+C and LJ+SC refer to Lennard-Jones fluid and amphiphilic chains using ($k_{ik}=0\epsilon/\sigma^2$) or ($k_{ik}=30\epsilon/\sigma^2$); see Eqs. (1)–(5).

Model	No. loose chains	No. grafted chains	Coverage	Time steps
LJ+C	0	68	0.33	1000000
LJ+C	24	44	0.22	1150000
LJ+C	42	26	0.13	1275000
LJ+C	68	0	0	1185000
LJ+SC	0	68	0.33	1000000
LJ+SC	24	44	0.22	1350000
LJ+SC	42	26	0.13	1365000
LJ+SC	68	0	0	1325000

to a coverage of 33% and randomly placing solvent molecules in the pore region [which defines the region between the opposing walls and is given by $L_xL_yL_z$ (see Fig. 1)] resulting in a total density of $\rho=N/V=0.825$. N is the total number of particles (beads + solvent molecules) in the cell of volume V. At this statepoint, chains attached to opposing walls are separated by a solvent region (i.e., interfacial region between opposing brushes), which in the most extended conformation of the chains is of thickness of $1-2\sigma$. In the course of the study, chains are removed randomly from both walls, but keeping the number of chains at both walls identical. However, the disposition of chains at opposite walls can be different.

We have performed a series of simulations by removing chains from the wall and allowing them to reach their equilibrium conformation in the pore region. As shown schematically in Fig. 1, these chains are no longer tethered to the surface. The simulations were carried out at surface coverages of 0.33, 0.22, 0.13, and 0 corresponding to 0, 24, 42, and 68 free chains. It is important to note that we are not reporting the dynamics of the depletion, but the steady state properties of the depleted layers.

The shear rate is fixed at $\dot{\gamma}^*=0.0101$. In our previous study [53], this was the lowest shear rate we could apply to obtain accurate viscosity profiles across the slab. The separation of the walls was fixed at 33.8 Å throughout. Further simulation details are described in Ref. [53]. As summarized in Table I, simulations were run for approximately 10^6 steps with a time step of $\Delta t^\star=0.0025$ (approaching a time scale of ns).

III. RESULTS AND DISCUSSIONS

We have investigated two different model systems to study the effect of shearing off the surface-attached amphiphiles as the two surfaces slid past each other on the shear viscosity and friction coefficient. The first model consists of amphiphilic molecules tethered to the wall and surrounded by solvent molecules. We will refer to this system as LJ+C (Lennard-Jones plus chains). In the second model, we increased the stiffness of the chains by including an additional harmonic potential [Eq. (5)]. We will refer to this model as LJ+SC (Lennard-Jones plus stiff chains). For both model systems, four different coverages 0.33 (0), 0.22 (24), 0.13 (42), and 0 (68) were studied, where the number in parentheses refers to the number of free chains. In the following discussion, we will introduce an abbreviation for convenience and indicate the coverage by placing the number of free chains after LJ+C or LJ+SC; e.g., at a coverage of 0.13 for the LJ+C system, we would write LJ+C42.

The shear field imposed by sliding the wall particles in opposite directions results in characteristic gradients in temperature, density, velocity, and viscosity, which will be addressed in the following discussion. The evolution of the temperature was monitored by calculating an average slab temperature defined as

$$T_z(z_n)=\left\langle \frac{\Sigma_{i=1}^{N} H_n(z_i) m_i [v_{z,i}-u_z(z_n)]^2}{k_B \Sigma_{i=1}^{N} H_n(z_i)} \right\rangle, \tag{7}$$

where the slab width for sampling was $\triangle z=1.2\sigma$. A detailed discussion of the effect of the slab width on the accuracy of the temperature is given in [53]. In Eq. (7), $\langle \cdots \rangle$ denotes a time average, m_i is the mass of particle i located in the slab n, and $H_n(z_i(t))$ is a top-hat function with functional values of

$$H_n(z_i)=1 \quad \text{for } z_n-\frac{\triangle z}{2}<z_i<z_n+\frac{\triangle z}{2}, \tag{8}$$

$$H_n(z_i)=0 \quad \text{otherwise.} \tag{9}$$

$u_z(z_n,t)$ in Eq. (7) is the instantaneous slab velocity in the z directions computed as $\Sigma_{i=1}^{N} H_n(z_i(t)) v_{z,i}(t)/N_n$, where $N_n=\Sigma_{i=1}^{N} H_n(z_i(t))$. Figure 2 shows the temperature profiles at different coverages for the LJ+C model. At all coverages, the conduction across the boundary is sufficiently fast that the fluid maintains the same temperature as the thermostated atoms in the walls. Only at zero coverage is a slight temperature increase observed, which, as discussed below, is due to a slip at the boundary. Similar results were obtained for the LC+SC model, where the temperature rise, as shown in Table II, is marginally higher at the different coverages.

The most important quantities in studying boundary lubrications by amphiphiles are the normal and tangential forces between the sliding coated surfaces, since these forces are a measure of the friction coefficient [59] defined as

$$\xi=\frac{-P_{xz}}{P_{zz}}. \tag{10}$$

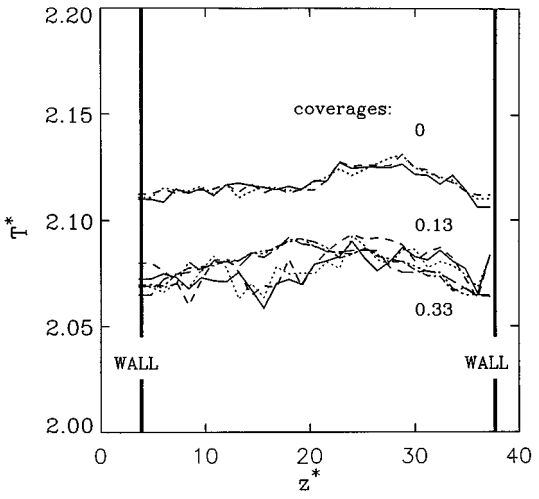

FIG. 2. Temperature profiles of the three components across the slab at distinct coverages for the system containing flexible amphiphilic molecules (LJ+C). The shear rate is $\dot{\gamma}^*=0.0101$. Quantities are given in reduced units, where $x^*=x/\sigma$, $y^*=y/\sigma$, $z^*=z/\sigma$, $T^*=k_BT/\epsilon$, and $\dot{\gamma}^*=\dot{\gamma}\sqrt{(m\sigma^2/\epsilon)}$.

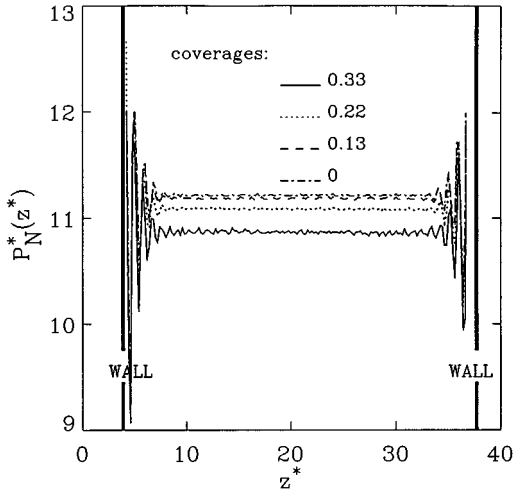

FIG. 3. Normal pressure tensor component profiles, $P_N^*(z^*)=P_N\sigma^3/\epsilon(z/\sigma)$, at different coverages computed during the simulations of the (LJ+C) system. See Fig. 2 for more details.

The off-diagonal pressure tensor component in the shear direction can also be used to calculate the viscosity,

$$\eta(z)=\frac{\langle -P_{xz}(z)\rangle}{\dot{\gamma}(z)}, \tag{11}$$

where the instantaneous shear rate, $\dot{\gamma}(z)$, is given by the velocity gradient, $du_x(z)/dz$. As in our previous study [53], we used the Irving-Kirkwood definition of the pressure tensor [60–62] to compute the stress across the pore.

$$\overline{\overline{\mathbf{P}}}(z)=\rho(z)k_BT\overline{\overline{\mathbf{I}}} - \frac{1}{L_xL_y}\left\langle \sum_{i<j}\frac{\vec{r}_{ij}\vec{r}_{ij}}{|\vec{r}_{ij}|}\frac{dU}{dr_{ij}}\frac{1}{|z_{ij}|}\bar{\theta}\left(\frac{z-z_i}{z_{ij}}\right)\bar{\theta}\left(\frac{z_j-z}{z_{ij}}\right)\right\rangle. \tag{12}$$

$\mathbf{I}$ is the unit tensor, $\langle\ \rangle$ denotes a configurational average, and $\bar{\theta}$ is a unit step function, which is 1 for every positive value of its argument and 0 otherwise. Details of the sampling procedure are given in [53]. Todd *et al.* [63] have recently pointed out that Eq. (12) is the leading order term in a series containing the expansion of the differential operator $O_{ij}=1\cdots+(1/n)[-\mathbf{r}_{ij}\cdot\partial/\partial\mathbf{r}]^{n-1}+\cdots$, (the IK1 approximation of [63]). The neglect of the higher order terms produces oscillations in the density profile close to the wall but does not significantly effect the estimates of the normal pressure from the fluid in the center of the box. The pressure tensor components, $P_{zz}(z)$ and $P_{xz}(z)$, at different coverages for the LJ+C model are displayed in Figs. 3 and 4, respectively. The constant values of the normal component over the fluid region are an indication that the system is mechanically stable [64]. Oscillations occurring close to the wall are due to the neglect of the higher order terms in the full Irving-Kirkwood expression [63]. An increase in $P_N(z)=P_{zz}(z)$ is observed as the coverage is reduced. However, the most significant changes are found between a coverage of 0.33 and 0.22, and the differences in $P_N(z)$ diminishes with decreasing coverages. Interestingly, not only does $P_{xz}(z)$ (shown in Fig. 4) become more negative for the intermediate coverages, but it also has approximately the same values for coverages of 0.33 and 0 as well as 0.22 and 0.13; see Table II. Figure 5 shows the friction coefficient calculated from Eq. (10), and, as indicated by the $P_{xz}(z)$ profiles, the frictional

TABLE II. Selected thermodynamic data taken at z', where the streaming velocity is zero; $v_x(z')=0$. See Table I for more details.

Model	Coverage	$\frac{dv^*}{dz^*}(z')$	$T^*(z')$	$P_N^*(z')$	$-P_{xz}^*(z')$	$\xi=\frac{\lvert P_{xz}\rvert}{P_{zz}}$	$\eta^*(z')$
LJ+C	0.33	0.039	2.07	10.87	0.047	0.0043	1.20
LJ+C	0.22	0.022	2.08	11.09	0.071	0.0064	3.19
LJ+C	0.13	0.019	2.09	11.19	0.073	0.0065	3.91
LJ+C	0	0.008	2.12	11.21	0.046	0.0041	5.70
LJ+SC	0.33	0.050	2.05	10.98	0.058	0.0060	1.14
LJ+SC	0.22	0.032	2.09	11.35	0.101	0.0095	3.21
LJ+SC	0.13	0.022	2.10	11.43	0.105	0.0094	4.86
LJ+SC	0	0.005	2.15	11.36	0.063	0.0053	8.44

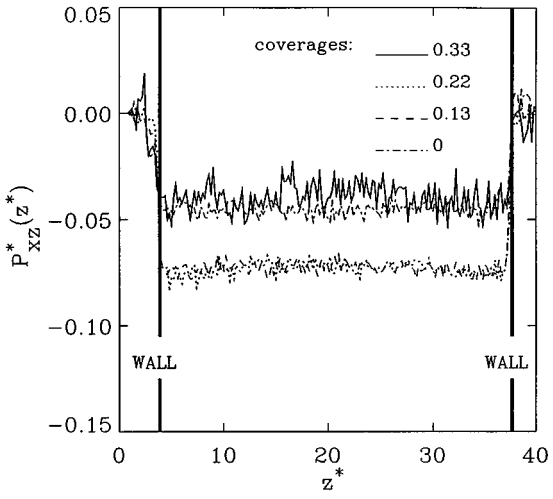

FIG. 4. Off-diagonal pressure tensor component profiles, $P^*_{xz}(z^*)$, at different coverages computed during the simulation of the (LJ+C) system. Quantities are expressed in reduced units. See Fig. 2 for more details.

forces for the intermediate coverages are higher than those found for coverages of 0.33 and 0. It is important to note that only at intermediate coverages are there grafted and free chains in the pore region, and it is the resulting entanglements between the grafted and free chains that increase the frictional forces. This effect is more pronounced for the LJ+SC model, where the stiffness of the chains is increased and the chains cannot easily adapt to changes in the fluid flow.

Velocity profiles for the LJ+C model system as a function of coverage are shown in Fig. 6. At coverages ranging from 0.33 to 0.13, the chains behave as if they were part of the wall and the sharp change in the velocity only occurs in the fluid region. This may be caused by the increased solvent density in the chain region close to the interface (see density profiles). Essentially solvent molecules are trapped between the chains reducing the flexibility of the amphiphilic mol-

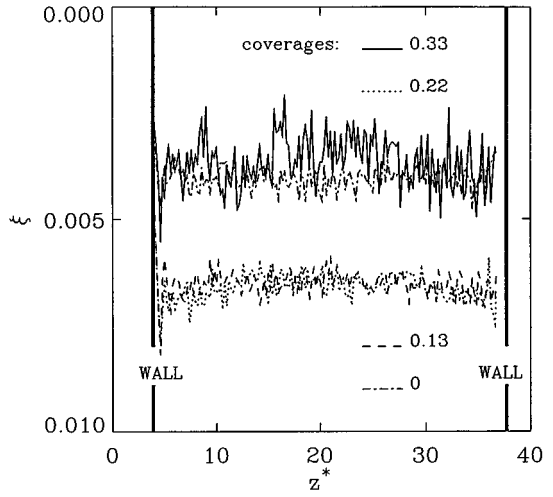

FIG. 5. Friction coefficients, $\xi = -P_{xz}/P_{zz}$, calculated across the slab for the (LJ+C) system at distinct coverages. Quantities are expressed in reduced units. See Figs. 2 and 3 for more details.

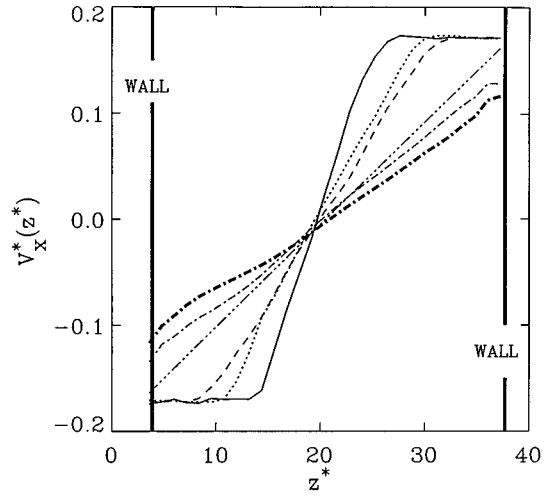

FIG. 6. Velocity profiles calculated across the slab are presented for 0.33 coverage (LJ+C) ——, 0.22 coverage (LJ+C) . . . . . , 0.13 coverage (LJ+C) – – – – – –, 0 coverage (LJ+C and LJ+SC; thicker line refers to LJ+SC) · – · – · – ·, and pure Lennard-Jones fluid · · · – · · · – · · ·. Quantities are given in reduced units. See Figs. 2 and 3 for more details.

ecules. Decreasing the coverage, the interfacial region becomes more diffuse and the profiles less steep. At a coverage of 0, a clear slip is visible causing the slight temperature rise observed in Fig. 1. For comparison, the velocity profile of a pure Lennard-Jones (LJ) fluid is also shown. The LJ fluid does not show a significant slip at the wall, which may demonstrate that increasing the chain length of the fluid increases the slip at the wall and, hence, reduces the heat conduction between fluid and wall. Similar profiles are obtained for the LJ+SC model. The profile for the LJ+SC0 system is significantly steeper than the one obtained for the LJ+C0 model, which is caused by the stiffness of the chain. For the LJ +SC0 system, the chains extend further into the fluid region, and essentially the fluid region becomes smaller (i.e., the hydrodynamic thickness of the LJ+SC0 layer is greater than for the LJ+C0 layer). Decreasing the coverage, the differences diminish and similar velocity gradients are found for a coverage of 0.13. At zero coverage, the slip at the wall is slightly larger for the LJ+SC model than for the LJ+C system. This is an indication that momentum flux is reduced due to the stiffness of the chains, which hinders the ability of the chains to adapt easily to changes in the flow pattern.

The average stress and the velocity profiles can be used to calculate the viscosity profiles using Eq. (11). These profiles as a function of coverages are displayed in Figs. 7 and 8 for the two models LJ+C and LJ+SC, respectively. The viscosity profile obtained for a pure LJ fluid [53] is also included in the figures for comparison. In the middle of the pore, the viscosities of LJ+C0 and LJ+SC0 are a factor of ≈ 2 lower than those of the LJ fluid. This is caused by the much steeper velocity profiles observed in the LJ+C and LJ+SC systems (see Fig. 6). Interestingly, the viscosities for the intermediate coverages are similar for the LJ+C system, whereas increasing the stiffness of the chains (LJ+SC) yields different values of the viscosity. In both model systems, the most dramatic change occurs between coverages of 0.13 and 0, where the latter model resembles an alkane-solvent mixture. The

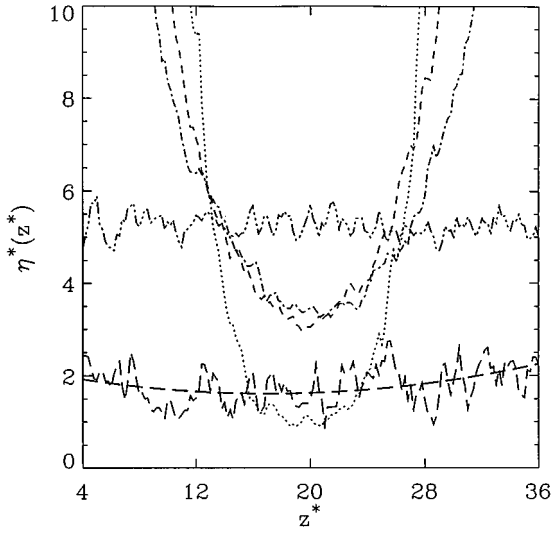

FIG. 7. Viscosity profiles calculated across the slab for the (LJ+C) system are presented for 0.33 coverage · · · · · · · · · · · ·, 0.22 coverage − − − − − −, 0.13 coverage · − · − · − ·, 0 coverage · · · − · · · − · · ·, and pure Lennard-Jones fluid — — — —. Quantities are given in reduced units. See Figs. 2 and 3 for more details.

viscosity of the LJ+SC68 model is higher than the one determined for the LJ+C68 system reflecting the stiffness of the chains. The same trend was observed for the friction coefficients (see Fig. 5 and Table II), which were larger for the LJ+SC model. However, approximately the same friction coefficients were determined for coverages of 0.33 and 0, whereas the viscosities for these two statepoints are significantly different.

Structural ordering of the different particles in the system was determined from the instantaneous number density in the slab n,

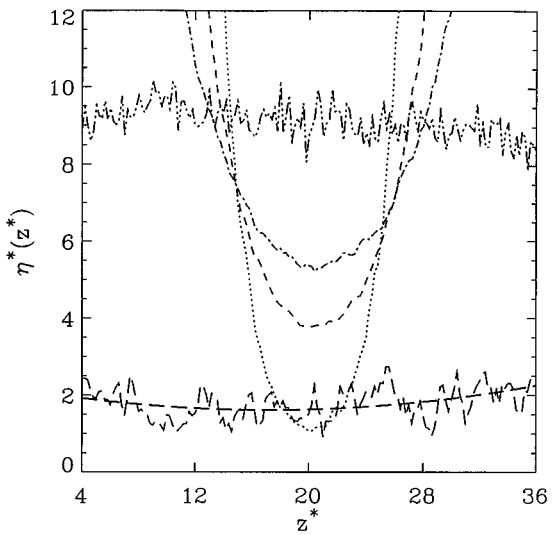

FIG. 8. Viscosity profiles calculated across the slab for the (LJ +SC) system are presented for 0.33 coverage · · · · · · · · · · · ·, 0.22 coverage − − − − − −, 0.13 coverage · − · − · − ·, 0 coverage · · · − · · · − · · ·, and pure Lennard-Jones fluid — — — —. Quantities are given in reduced units. See Figs. 2 and 3 for more details.

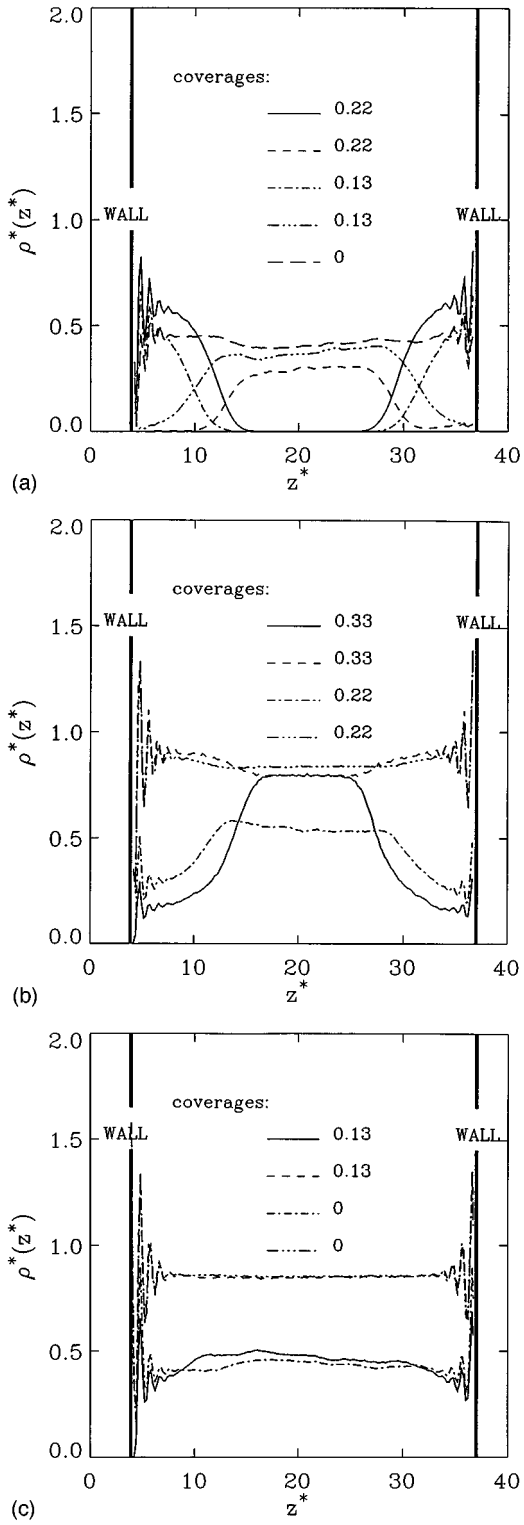

FIG. 9. (a) Density profiles, $\rho^*(z^*)=\rho\sigma^3(z/\sigma)$, of the grafted (———— and · − ·) and loose (− − −, · · · − · · ·, and — — — —) chains computed across the slab for the (LJ+C) system. Quantities are given in reduced units. (b) Profiles of the total (− − − and · · · − · · ·) and fluid (—— and · − ·) densities computed across the slab for the (LJ+C) system at different coverages. (c) Profiles of the total and fluid densities computed across the slab for the (LJ+C) system at different coverages.

TABLE III. Radius of gyration. See Table I for more details.

Model	No. grafted chains	$\langle S^2_{tot}\rangle$ (free)	$\langle S^2_{\perp}\rangle$ (free)	$\langle S^2_{\parallel}\rangle$ (free)	$\langle S^2_{tot}\rangle$ (grafted)	$\langle S^2_{\perp}\rangle$ (grafted)	$\langle S^2_{\parallel}\rangle$ (grafted)
LJ+C	68	—	—	—			
LJ+C	44	5.8	1.6	4.2	7.7	4.9	2.8
LJ+C	26	5.5	1.5	4.0	6.6	3.0	3.6
LJ+C	0	5.2	1.6	3.7	—	—	—
LJ+SC	68	—	—	—			
LJ+SC	44	11.0	2.2	8.9	13.2	7.1	6.1
LJ+SC	26	10.9	2.3	8.7	13.2	9.0	4.2
LJ+SC	0	10.4	2.7	7.7	—	—	—

$$\rho(z_n)=\left\langle \frac{1}{L_x L_y \triangle z}\sum_{i=1}^{N} H_n(z_i)\right\rangle. \tag{13}$$

The same slab width, $\triangle z$, and sampling procedure were applied in the simulations as in [53]. Figures 9(a)–9(c) show the different density profiles determined during the simulations of the LJ+C model. Figure 9(a) displays the profiles for grafted and free amphiphiles at distinct coverages. At high coverage, the overlap between the profiles for grafted and free chains is small, indicating only a small penetration depth of the free chains into the grafted layer. Larger penetration is observed for the coverage of 0.13, where the overlap of the profiles is substantial. At a coverage of 0, as expected, the density profile is constant across the pore. Histograms for the solvent particles and all particles in the system as a function of coverage are shown in Figs. 9(b) and 9(c). At the highest coverage of 0.33, the penetration of solvent molecules into the chain region decreases towards the wall. Lowering the coverage significantly increases the possibility of solvent molecules entering the chain region, and at a coverage of 0.13 the fluid density is approximately constant across the slab. The small decrease in density close to the wall reflects the limited space due to grafted amphiphiles.

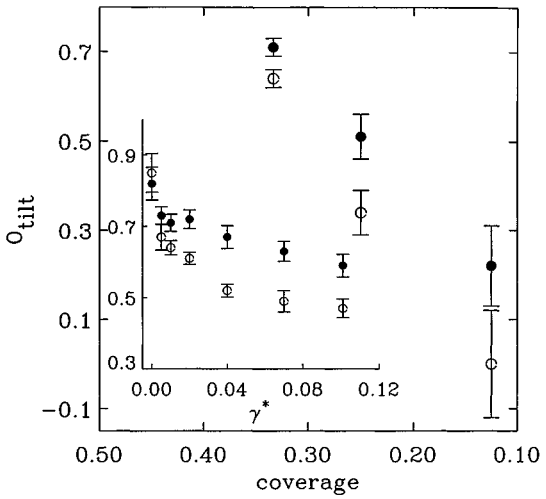

FIG. 10. Tilt order parameter of the grafted chains calculated during the simulation of the two different model systems LJ+C (●) and LJ+SC (○) as a function of shear rate and coverage. Quantities are given in reduced units. See Fig. 2 for more details.

In the case of the LJ+SC system (results not shown), the observations are qualitatively similar, but more solvent molecules penetrate the region of grafted amphiphiles at high coverages, and the width of the density profiles for the

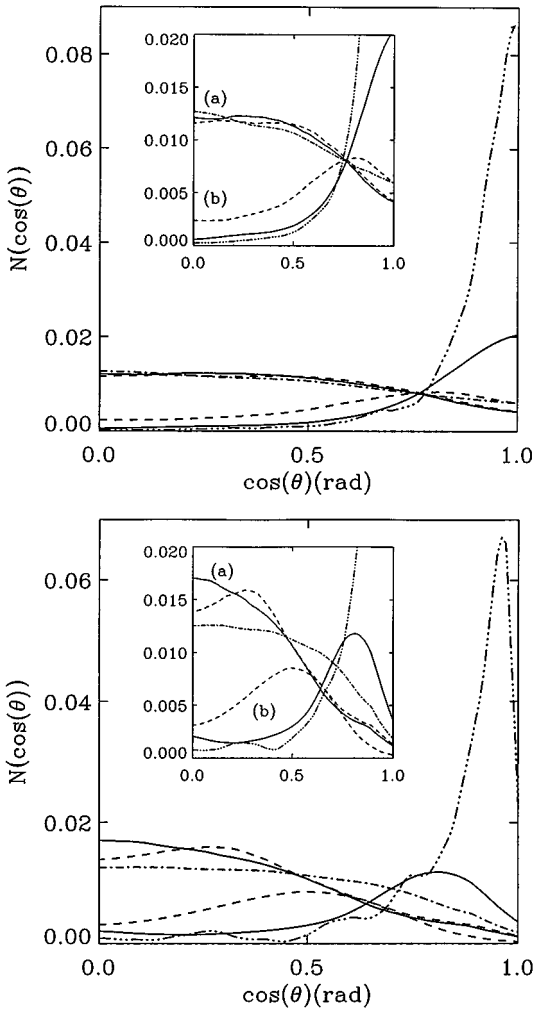

FIG. 11. (a) Tilt distribution of (a) loose and (b) grafted chains determined during the simulations of the model system (LJ+C). Coverages are 0.33 · · · − · · · − · · ·, 0.22 ——, 0.13 − − − − − −, and 0 · − · − · − · − ·. (b) Tilt distribution of (a) loose and (b) grafted chains determined during the simulations of the model system (LJ+SC). Coverages are 0.33 · · · − · · · − · · ·, 0.22 ——, 0.13 − − − − − −, and 0 · − · − · − · − ·.

grafted chains extends further into the fluid region than the ones obtained for the LJ+C system, reflecting the stiffness of the chains.

Complementary information about the conformation of the chains and their alignment in the flow was deduced from the radii of gyration [65,66] given in Table III, tilt order parameter displayed in Fig. 10 and tilt distributions shown in Figs. 11(a) and 11(b). The mean square radius of gyration and its components [65,66] were computed as

$$\langle S_{\parallel}^2 \rangle = \frac{1}{N} \sum_{k=1}^{N} \langle (x_k - x_{\mathrm{com}})^2 + (y_k - y_{\mathrm{com}})^2 \rangle, \tag{14}$$

$$\langle S_{\perp}^2 \rangle = \frac{1}{N} \sum_{k=1}^{N} \langle (z_k - z_{\mathrm{com}})^2 \rangle, \tag{15}$$

$$\langle S_{\mathrm{tot}}^2 \rangle = \langle S_{\parallel}^2 \rangle + \langle S_{\perp}^2 \rangle, \tag{16}$$

where the index ''com'' refers to the center of mass of each chain. The tilt angle was determined as the angle between the surface normal of the boundary (see Fig. 1) and the long axis of the molecule, which is defined as that eigenvalue of the inertia moment tensor with the smallest eigenvector. Reducing the coverage has only a marginal effect on the conformation of the free chains: the $S_{\perp}^2$ and $S_{\parallel}^2$ values are presented in Table III. The grafted chains are more sensitive to changes in surface coverage. For both models, $S_{\parallel}^2$ increases and $S_{\perp}^2$ decreases as the coverage is reduced, which is an indication that the tilt angle increases. As one would expect, the changes observed in both components are more significant in the LJ+SC system. Compared with the LJ+C model, both $S_{\perp}^2$ and $S_{\parallel}^2$ increase for the LJ+SC system, suggesting that the tilt is accommodated by a stretching of the chains. The tilt behavior is also observed from the tilt order parameters shown in Fig. 10. Increasing the stiffness of the amphiphilic molecules yields a larger tilt, indicating that the stiff chains are more sensitive to the induced shear stress. A more flexible chain has an additional degree of freedom in folding, essentially reducing $S_{\perp}^2$. The inset in Fig. 10 shows the tilt order parameter as a function of shear rate taken from Ref. [53]. Lowering the coverage, it has a much more pronounced effect on the tilt behavior than increasing the shear rate by a factor of 10. Tilt distributions of the grafted and free chains for the LJ+C and LJ+SC models are displayed in Figs. 11(a) and 11(b), respectively. As already indicated by the order parameters and radii of gyration, the grafted chains are more sensitive to changes in coverages than the free chains. At all coverages, the free chains show a tendency to align with the fluid to the same extent indicated by the broadness and similarity of the distributions. Stiffer chains align more with the fluid than the flexible ones to reduce the flow resistance. For the grafted amphiphiles (LJ+SC) the distributions are shifted further to smaller angles than observed for the LJ+C model.

IV. CONCLUSIONS

We have performed nonequilibrium molecular dynamics simulations to examine the rheological and structural properties of a complex fluid system composed of solvent molecules, grafted and free amphiphiles. In our previous study [53], we focused our investigations on a relatively low surface coverage and examined the interplay between solvent and amphiphiles as a function of shear rate. Here, we have maintained a constant low shear rate throughout the simulations and varied the surface coverage from 0.33 to 0 by randomly detaching amphiphiles from the wall. The reduced shear rate is 0.0101, which in our previous study was the lowest shear rate we could apply to compute reliable stress and viscosity data.

As observed previously [53], the grafted chains behave like a wall at coverages larger than 0. For a pure amphiphile-solvent mixture (coverage 0), a slip evolves at the boundary, which is more pronounced for the stiffer surfactants. A key parameter in boundary lubrication processes is the friction coefficient. For the LJ+C and LJ+SC models, the coefficients are constant across the pore at all coverages studied. Surprisingly, the frictional forces for the intermediate coverages are higher than those found for coverages of 0.33 and 0. We note that only at intermediate coverages are there grafted and free chains in the pore region. It appears as if entanglements between grafted and free chains, which are indicated by the overlap of the corresponding density profiles, increase the frictional force. This effect is more pronounced for the LJ+SC model, where the chains are less flexible and, hence, the amphiphile cannot easily adapt to changes in the fluid flow. This is also reflected in the geometrical quantities for the grafted amphiphiles, where the stiffer chains are more tilted and stretched due to the flow resistance. The structural ordering of the free chains are independent of coverage, and have the tendency to align with the fluid flow, which due to the stiffness of the amphiphiles is more pronounced for the LJ+SC model.

ACKNOWLEDGMENTS

Computations were performed at the University of Southampton and at Novo-Nordisk A/S. G.H.P. would like to acknowledge financial support from the European grants CHRX CT 930092/190 and BIOZ-CT93-5507. D.J.T. would like to thank the EPSRC for a grant GR/J/74459 for computing equipment.

[1] H. Yoshizawa, Y.-L. Chen, and J. Israelachvili, J. Phys. Chem. **97**, 4128 (1993).

[2] H. Yoshizawa and J. Israelachvili, J. Phys. Chem. **97**, 11 300 (1993).

[3] P. A. Thompson and M. O. Robbins, Science **250**, 792 (1990).

[4] V. Schmitt, F. Lequeux, A. Pousse, and D. Roux, Langmuir **10**, 955 (1994).

[5] M. L. Gee, P. M. McGuiggan, J. Israelachvili, and A. M. Homola, J. Chem. Phys. **93**, 1895 (1990).

[6] R. G. Horn, S. J. Hirz, G. Hadziioannou, C. W. Frank, and J.

M. Catala, J. Chem. Phys. **90**, 6767 (1989).
[7] J. Van Alsten and S. Granick, Phys. Rev. Lett. **61**, 2570 (1991).
[8] J. Klein, E. Kumacheva, D. Mahalu, D. Perahia, and L. J. Fetters, Nature **370**, 634 (1994).
[9] H.-W. Hu and S. Granick, Science **258**, 1339 (1992).
[10] R. G. Horn, J. N. Israelachivili, and F. Pribac, J. Coll. Interf. Sci. **115**, 480 (1987).
[11] U. Landman, W. D. Luedtke, N. A. Burnham, and R. J. Colton, Science **248**, 454 (1990).
[12] U. Landman, W. D. Luedtke, and E. M. Ringer, Wear **153**, 3 (1992).
[13] J. N. Israelachivili, *Intermolecular and Surface Forces* (Academic Press, London, 1992).
[14] A. W. Adamson, *Physical Chemistry of Surfaces* (Wiley, New York, 1982).
[15] J. R. Smith, G. Bozzolo, A. Banerjea, and L. Ferrante, Phys. Rev. Lett. **63**, 1269 (1989).
[16] M. W. Ribarsky and U. Landman, Phys. Rev. B **38**, 9522 (1988).
[17] E. Rabinowicz, *Friction and Wear of Materials* (Wiley, New York, 1965).
[18] C. W. Mate, G. M. McClelland, R. Erlandsson, and S. Chiang, Phys. Rev. Lett. **59**, 1942 (1987).
[19] K. K. Han, J. H. Cushman, and D. J. Diestler, Mol. Phys. **79**, 537 (1993).
[20] Y. Wang, K. Hill, and J. G. Harris, J. Chem. Phys. **100**, 3276 (1994).
[21] S. R. Cohen, G. Neubauer, and G. M. McClelland, J. Vac. Sci. Technol. A **8**, 3449 (1990).
[22] G. M. McLelland, *Adhesion and Friction* (Springer, Berlin, 1989).
[23] B. N. J. Persson, Phys. Rev. Lett. **71**, 1212 (1993).
[24] P. A. Thompson and M. O. Robbins, Phys. Rev. A **41**, 6830 (1990).
[25] S. Y. Liem, D. Brown, and J. H. R. Clarke, Phys. Rev. A **45**, 3706 (1992).
[26] Y. Liem, Ph.D. thesis, University of Manchester, Manchester, United Kingdom (1992).
[27] T. K. Xia, J. Ouyang, M. W. Ribarsky, and U. Landman, Phys. Rev. Lett. **69**, 1967 (1992).
[28] P. Padilla and S. Toxvaerd, J. Chem. Phys. **101**, 1490 (1994).
[29] J. B. Sokoloff, Phys. Rev. B **42**, 760 (1990).
[30] W. Zhong and D. Tomanek, Phys. Rev. Lett. **64**, 3054 (1990).
[31] J. A. Harrison, C. T. White, R. J. Colton, and D. Brenner, Phys. Rev. B **46**, 9700 (1992).
[32] J. A. Harrison, C. T. White, R. J. Colton, and D. Brenner, J. Phys. Chem. **97**, 6573 (1993).
[33] J. N. Glosli and G. M. McClelland, Phys. Rev. Lett. **70**, 1960 (1993).
[34] Y. H. Kim, J. T. Nelson, and B. Glynn, Cereal Foods World **39**, 8 (1994).
[35] P. G. Gennes, Macromolecules **13**, 1069 (1980).
[36] P. G. Gennes, *Scaling Concepts in Polymer Physics* (Cornell Univ. Press, Cornell, 1979).
[37] A. Baumgärtner, in *Application of the Monte Carlo Method in Statistical Physics*, edited by K. Binder (Springer, Berlin, 1984).
[38] K. Binder, *Computational Modeling of Polymers* (J. Biorano, New York, 1992).
[39] R. J. Roe, *Computer Simulations of Polymers* (Prentice Hall, Englewood Cliffs, NJ, 1991).
[40] K. Binder, *Monte Carlo Methods in Statistical Physics* (Springer, Berlin, 1979).
[41] D. J. Diestler, M. Schoen, and J. H. Cushman, Science **262**, 545 (1993).
[42] J. Atkinson, C. J. Goh, and N. Phan-Thien, J. Chem. Phys. **80**, 6305 (1984).
[43] P.-Y. Lai and K. Binder, J. Chem. Phys. **98**, 2366 (1993).
[44] G. S. Grest and K. Kremer, Phys. Rev. A **33**, 3628 (1986).
[45] K. Kremer and G. S. Grest, J. Chem. Phys. **92**, 5057 (1990).
[46] K. Kremer and G. S. Grest, *Computer Simulations of Polymers* (Prentice Hall, Englewood Cliffs, NJ, 1991).
[47] K. Kremer, in *Computer Simulation in Chemical Physics*, edited by M. P. Allen and D. J. Tildesley, Vol. 397 of NATO Advanced Study Institute Series C: Mathematical and Physical Science (Kluwer Academic Publishers, London, 1993).
[48] M. Murat and G. S. Grest, Phys. Rev. Lett. **63**, 1074 (1989).
[49] K. J. Chugg, Ph.D. thesis, St Edmunds College, Cambridge, United Kingdom (1990).
[50] E. Evans and A. Yeung, Chem. Phys. Lip. **73**, 39 (1994).
[51] J. D. Weeks, D. Chandler, and H. C. Andersen, J. Chem. Phys. **54**, 5237 (1971).
[52] M. P. Allen and D. J. Tildesley, *Computer Simulation of Liquids* (Clarendon, Oxford, 1989).
[53] G. H. Peters and D. J. Tildesley, Phys. Rev. E **52**, 1882 (1995).
[54] W. G. Hoover, *Molecular Dynamics* (Springer, Berlin, 1987).
[55] D. J. Evans and G. P. Morriss, *Statistical Mechanics of Nonequilibrium Liquids* (Academic, London, 1990).
[56] W. G. Hoover, Phys. Rev. A **31**, 1695 (1985).
[57] W. G. Hoover, D. J. Evans, R. B. Hickman, A. J. C. Ladd, W. T. Ashurst, and B. Moran, Phys. Rev. A **22**, 1690 (1980).
[58] D. J. Evans and G. P. Morriss, Phys. Rev. A **30**, 1528 (1984).
[59] H. A. Barnes, J. F. Hutton, and K. Walters, *An Introduction to Rheology* (Elsevier, Amsterdam, 1989).
[60] J. P. R. B. Walton, D. J. Tildesley, and J. S. Rowlinson, Mol. Phys. **48**, 1357 (1983).
[61] J. P. R. B. Walton, D. J. Tildesley, and J. S. Rowlinson, Mol. Phys. **58**, 1013 (1986).
[62] D. H. Tsai, J. Chem. Phys. **70**, 1375 (1979).
[63] B. D. Todd, D. J. Evans, and P. J. Daivis, Phys. Rev. E **52**, 1627 (1995).
[64] J. S. Rowlinson and B. Widom, *Molecular Theory of Capillarity* (Clarendon Press, Oxford, 1989).
[65] P. J. Flory, *Statistical Mechanics of Chain Molecules* (Interscience Publishers, New York, 1986).
[66] M. Doi and S. F. Edwards, *The Theory of Polymer Dynamics* (Clarendon Press, Oxford, 1986).